ChemComm

Highly active, selective and stable hollow nanocarbon supported Pd particles for selective hydrogenation of 3-nitrostyrene

Journal:	*ChemComm*
Manuscript ID	CC-COM-09-2018-007430.R1
Article Type:	Communication

ChemComm

COMMUNICATION

Highly active, selective and stable hollow nanocarbon supported Pd particles for selective hydrogenation of 3-nitrostyrene

Yang Lou, Jia Xu, Honglu Wu, Jingyue Liu*

2Received 00th January 20xx,
Accepted 00th January 20xx

DOI: 10.1039/x0xx00000x

www.rsc.org/

Constructing Pd-C bonds between Pd particles and highly defective hollow nanocarbons (h-NCs) not only enables facile H_2 dissociation but also the diffusion of the dissociated H species, which makes the synthesized Pd/h-NC catalyst highly active with a TOF of 21, 845 /h (>80 times higher than that on the best catalyst reported in literature), selective (97%), and stable (4 cycles) for selective hydrogenation of 3-nitrostyrene to 3-ethylnitrobenze.

Catalytic hydrogenation is considered as an environmentally friendly and efficient process for hydrogenation of nitroarenes to produce versatile intermediates for production of dyes, pharmaceuticals, flavors, agrochemicals and polymers.[1-4] However, a catalyst that possesses both high activity and selectivity, especially in the presence of two or more reducible functional groups (e. g. selective hydrogenation of nitrostyrene), under mild reaction conditions is highly desirable. Most of the available supported metal catalysts cannot meet such a demanding goal of selective hydrogenation. For example, unmodified Pd-based catalysts normally lead to overly hydrogenated products attributable to the strong hydrogenation ability of Pd particles.[5-7] For selective hydrogenation of targeted molecules and products, one needs to consider both the H_2 activation process and the adsorption strength of dissociated H atoms on the surfaces of the active species.[8, 9] A catalyst that possesses facile activation of H_2 and weak adsorption of the dissociated H atoms can exhibit optimal efficiency in balancing activity and selectivity for the targeted product.[8, 10] The electronic properties of active metal species play a crucial role in determining the adsorption behavior of functional groups and the dissociation behavior of H_2.[3, 5, 11] Hence, how to efficiently tune the electronic properties of active species/sites is critical to enhancing a catalyst's overall performance for selective hydrogenation reactions.

The use of transition metals or other types of additives to modify the electronic structure of active sites can enhance selectivity but at the expense of activity.[11-13] For example, the addition of alkali ions enables modulating the electronic properties of supported active metal species, which controls the activity and selectivity for 3-nitrostyrene hydrogenation.[11] Metal alloying is considered another efficient method to tune the electronic properties of active metal species and correspondingly enhance their catalytic performance. [8, 9, 14] Another approach is to choose the appropriate reducible oxides as supports that can influence the catalytic activity and selectivity of the active phases via strong metal-support interactions.[1, 15, 16]

For liquid phase reactions, carbon supports have been widely used because of their high chemical stability in either acid or base solvents, high mechanical stability, high total surface area, and unique electronic properties.[17, 18] Graphitic carbon materials are generally not appropriate for anchoring metal species, especially noble metals, due to the chemical inertness of the graphite basal planes.[19] Therefore, strategies for engineering defects (e.g., topological, dangling bonds, rehybridization and other types of defects[20, 21]) of, introducing functional groups to, and/or incorporating heteroatoms in, carbon structures have been proposed to strengthen the electronic interaction between active metal species and the functional moieties or defects on carbon surfaces.[21, 22] In this work, we propose a new strategy to enhance the catalytic activity and selectivity for selective hydrogenation reactions: constructing strong metal-carbon bonding to finely tune the electronic structure of active metal species through strong electronic interaction between metal particles and edge/defect sites of carbon supports.

In this present study, we fabricated hollow nanocarbons (h-NCs) that possess high number density of surface edge/defect sites, high total surface area, and highly accessible mesopores. Our concurrent research work has confirmed that these edge/defect sites of the synthesized h-NCs efficiently modulate the electronic structure of anchored single Pt atoms and significantly enhance their chemical reactivity. We hypothesize that strong interaction between small Pd clusters and the carbon edge atoms forming Pd-C bonds can tune the hydrogenation ability of the Pd clusters to a degree that both the H_2 dissociation and the adsorption of the dissociated H atoms are appropriate for the targeted selective hydrogenation of 3-nitrostyrene to 3-ethylnitrobenze with high activity and selectivity.

Department of Physics, Arizona State University, Tempe, Arizona 85287, United States
E-mail: jingyue.liu@asu.edu
Electronic Supplementary Information (ESI) available: [Experimental details, HAADF-STEM images of h-NCs and Pd_1/h-NC SAC; Defect density, Raman and XPS spectra of Pd/HC and Pd/XC-72 catalysts; Activity and selectivity comparison with other published catalysts]. See DOI: 10.1039/x0xx00000x

Our experimental results demonstrate that the synthesized h-NCs supported Pd particles are highly active and selective for the hydrogenation of 3-nitrostyrene to 3-ethylnitrobenze, under very mild reaction conditions (40 °C and 5 bar H_2) with ethanol as the reaction medium, with a selectivity of 97% and a turnover frequency (TOF) as high as 21, 845 per Pd atom per hour (21, 845 /h), more than 80 times higher than that of the best catalyst reported in literature.[23]

The h-NCs are synthesized by a template-assisted catalytic deposition and evaporation process by using ZnO nanowires as template (See sample preparation details in the supporting materials). The h-NCs possess a BET surface area of ~1,100 m^2/g and a tube morphology with inner diameters ranging from 20 to 100 nm and lengths ranging from 1 to 20 micrometers (Figure S1). The wall thicknesses of the h-NCs range from 2-5 nm with numerous mesopores (an average pose diameter of ~4.3 nm) on the side walls (Figure S2). The synthesized h-NCs consist of stacked hyper-cross-linked graphene sheets with sizes ranging from 0.5 to 3.1 nm, resulting in disordered and defective graphene-like structures (Figure S3). The presence of numerous edge sites in the synthesized h-NCs can be effectively utilized to anchor single metal atoms, clusters or nanoparticles.

The aberration-corrected high-angle annular dark-field scanning transmission electron microscopy (HAADF-STEM) imaging technique (Figure 1), indispensable for determining the dispersion of supported metal catalysts[24], was used to examine the spatial and size distribution of Pd particles supported on the h-NCs (denoted as Pd/h-NC with Pd loading of 0.49 wt.%): The Pd particles are uniformly distributed across the h-NCs with an average size of 2.8 ± 0.2 nm. To compare with literature results, the Vulcan XC-72 carbon, widely used in a variety of catalytic reactions[25], was used to synthesize a control catalyst. The XC-72 carbon, with a BET surface area of 254 m^2/g, consists of aggregated spherical particles with a compact, onion-like graphitic structure (Figure S4). The Pd particles supported on the XC-72 carbon powders (Figure 1b), denoted as Pd/XC-72 with a Pd loading of 0.58 wt.%, have slightly larger sizes with an average size of 3.1 ± 0.1 nm.

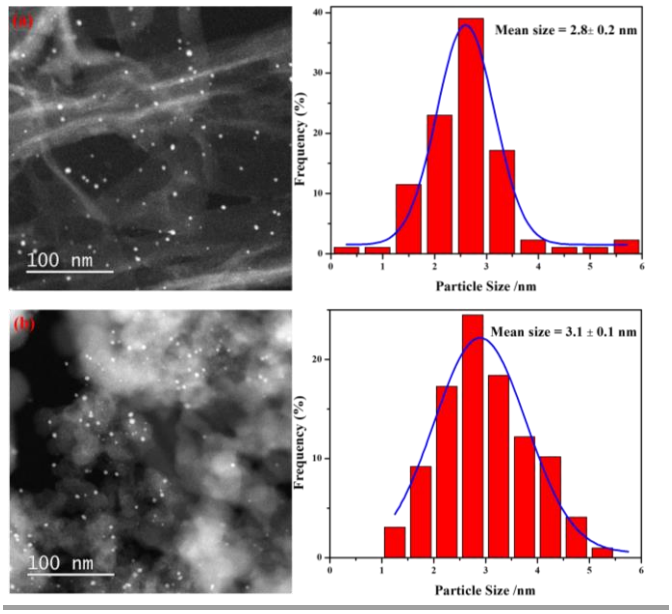

Figure 1. HAADF-STEM images and particle size distributions of fresh Pd/h-NC and Pd/XC-72.

As shown in Table 1, the synthesized Pd/h-NC is highly active for hydrogenation of 3-nitrostyrene with a selectivity of 97.0% toward 3-ethylnitrobenzene under mild reaction conditions (40 °C and 5 bar H_2). The 3-ethylaniline was the only by-product and hydroxylamine or other types of side products were not detectable. The catalyst maintained its selectivity (> 91%) toward 3-ethylnitrobenzene even after 4 cycles (Figure S5). Electron microscopy characterizations and metal analyses did not reveal recognizable sintering of Pd nanoparticles (Figure S6) or leaching of Pd during the catalytic reactions. The slight decrease in conversion rate during the stability test originated from the loss of catalyst powders during the filtering processes since we used only 5 mg catalysts for the hydrogenation reactions. The TOF of the Pd/h-NC was calculated to be 21, 845 /h, ~84 times higher than that of the best catalyst reported in literature.[23] The recently developed single-atom catalysts (SACs) normally exhibit high selectivity toward selective hydrogenation reactions due to the uniformity of isolated active sites.[26-30] However, when downsizing the Pd particles to single atoms (Figure S7) the Pd_1/h-NC SAC (with a Pd loading of 0.19 wt.%) exhibited a much lower selectivity toward 3-ethylnitrobenze (82.7%) under the same reaction conditions (Table 1) although the TOF was estimated to be 22,070 /h, similar to that of the Pd/h-NC catalyst. Compared to other highly selective catalysts for hydrogenation of 3-nitrostyrene (Table S1), the use of ethanol as the reaction medium, as practiced here on the synthesized Pd/h-NC, is much greener and more environmentally friendly than that by using toxic and/or environmentally unfriendly solvents such as heptane, toluene, and tetrahydrofuran as the reaction medium to enhance the catalytic selectivity of 3-nitrostyrene hydrogenation to 3-ethylnitrobenze.[4, 14, 23, 31, 32] The catalytic evaluation results indicate that the Pd/h-NC catalyst not only provides better performance but also enables catalytic transformation of important molecules in a more environmentally friendly reaction medium.

Table 1 Catalytic activity and selectivity of selective hydrogenation of 3-nirostyrene over carbon supported Pd catalysts[a]

Catalyst	Conversion /%	Selectivity /%			
		3-VA	3-EA	3-ENB	Other
Pd/h-NC	94.9	0	3.0	97.0	0
Pd/XC-72	12.8	7	12.8	80.2	0
10 wt.% Pd/C[b]	99.9	0	50.4	37.5	12.1
Pd_1/h-NC	24.2	3.7	13.7	82.7	0
Pure h-NC[c]	0	0	0	0	0
Pure XC-72[d]	0	0	0	0	0

a: Reaction conditions: 40 °C for 10 min, 5bar H_2 as hydrogen donor, 8 ml ethanol as reaction solvent, 0.33 mmol 3-nitrostyrene, Pd/substrate ratio is 0.14%. 3-VA: 3-vinylaniline; 3-EA: 3-ethylaniline; 3-ENB: 3-ethylnitrobenze.

b: Commercial 10 wt.% Pd/C from Sigma-Aldrich.

c: Reaction time is 60 min.

d: Reaction time is 30 min.

When different types of carbon supports were used the corresponding supported Pd catalysts exhibited much lower selectivity toward 3-ethylnitrobenzene (Table 1). For example, the commercial Pd/C catalyst (purchased from Sigma-Aldrich) yielded a selectivity of only 37.5% toward 3-ethylnitrobenzene and the reaction product was dominated by 3-ethylaniline. Furthermore, the total activity for hydrogenation of 3-nitrostyrene on the commercial Pd/C catalyst (TOF

= 8,768 /h) was much lower than on the Pd/h-NC. The selectivity toward 3-ethylnitrobenzene on the control Pd/XC-72 catalyst was 80.2% with a total TOF of 9,300 /h, ~ 2.3 times lower than that on the Pd/h-NC catalyst. The pure h-NCs and XC-72 carbon, under the same reaction conditions, were not active (Table 1). These results suggest that the physicochemical properties of the carbon supports play a significant role in determining both the selectivity and activity of selective hydrogenation of 3-nitrostyrene on carbon supported Pd nanoparticle catalysts.

In order to understand why the Pd/h-NC catalyst is more active and selective, we characterized this catalyst in detail. With similar Pd loading, the HAADF-STEM images show that the size and spatial distribution of the Pd particles are similar in both the Pd/h-NC and the Pd/XC-72 catalysts, suggesting that the size and shape of the Pd particles may not play a significant role in differentiating the performance of these two catalysts. The geometric and electronic properties of the carbon supports play an important role in stabilizing metal species and tuning their electronic properties.[33] Raman spectroscopy, capable of providing useful information on the density of defects in carbon materials, [34-36] was used to characterize the as-prepared h-NCs and the XC-72. The peak at 1591 cm^{-1} of the Raman spectra (Figure S8 and S9) is assigned to the G-band, corresponding to the bond stretch of all pairs of sp^2 in both carbon ring and chain and the peak at 1345 cm^{-1} is assigned to the D1-band, corresponding to the defects within the carbon structure.[37] The ratio between the D1 and G band intensities (I_{D1}/I_G) is used to quantify the degree of structural disorder in the carbon materials.[34] The I_{D1}/I_G value of the h-NCs was estimated to be ~1.1 while that of the XC-72 was estimated to be ~0.85 (Figure S7 and S8), suggesting that the defect density in the h-NCs is much higher.[38, 39] Based on the empirical formula models[40, 41], we estimated that the crystallite size (related to the amount of crystal boundary, including dislocations, vacancies and so on)[35] of the h-NCs (~6.6 nm) is much smaller than that of the XC-72 (~14.2 nm). Correspondingly, the defect density of the h-NCs is roughly 5 times higher than that of the XC-72 (Table S2). Both the atomic resolution STEM images and the Raman spectra confirm the existence of numerous edge defect sites in the synthesized h-NCs.

When the Pd particles were deposited on the h-NCs, the I_{D1}/I_G ratio dropped by ~19% (Figure S8) and the defect density dropped by ~20% (Table S2). The significant decrease in the I_{D1}/I_G ratio and the defect density is most probably a result of strong metal-support interaction: the Pd particles interacted with the edges/defects of the h-NCs to form strong Pd-carbon bonds. It has been reported that hybridization of the d orbitals of the Pd atoms with the s and p orbitals of the adjacent C atoms leads to strong electronic interaction and electron transfer from the Pd particles to the carbon support, resulting in positively charged Pd particles.[42-44] The strong edge anchoring of the Pd particles not only makes them stable during hydrogenation reactions but also tunes their catalytic properties to yield higher selectivity for hydrogenation of 3-nitrostyrene to 3-ethylnitrobenze.

When the Pd particles were deposited on the XC-72, the I_{D1}/I_G ratio dropped only slightly by ~1% compared to that of the pure XC-72 (Figure S9), suggesting that the deposition of the Pd particles did not significantly affect the carbon structure due to a weak interaction between them. The slight decrease (6 ~ 8%) of defect number density (Table S2) further indicates that the graphitic XC-72 carbon cannot efficiently bond with and anchor Pd particles, resulting in the lower stability of the Pd/XC-72 catalyst during selective hydrogenation of 3-nitrostyrene to 3-ethylnitrobenze.

In order to further unravel the electronic properties of the supported Pd nanoparticles, the X-ray photoelectron spectroscopy (XPS) experiments were conducted on the Pd/h-NC and Pd/XC-72 catalysts (Figure S10). After a deconvolution processing of the Pd $3d_{5/2}$ peak obtained on the Pd/XC-72, the two peaks located at 338.0 eV and 337.3 eV were assigned to the oxidation states of PdO_2 and PdO, respectively.[45, 46] For the Pd/h-NC catalyst, the two peaks are located at 337.9 eV (assignable to the PdO_2 species) and 337.0 eV. The peak at 337.0 eV, however, is between the values of Pd^{1+} (335.5 eV) and Pd^{2+} (337.3 eV).[47] Therefore, this peak can be attributed to the electron-depleted Pd atoms (Pd^{n+}, 1< n <2), resulting from electron transfer from the Pd species to the carbon support,[33] corroborating the Raman result (Figure S8). Under hydrogenation reaction conditions, the Pd oxide species can be easily reduced to metallic state and form PdH_x species[48], resulting in decrease of selectivity.[5] The carbon-bonded Pd species maintain their valence state due to charge transfer and the electron depletion induces downshift of the d-band center of the Pd^{n+} species and thus reduces the binding strength of the dissociatively adsorbed hydrogen.[5, 49] The weakly bound, active hydrogen species associated with the interfacial regions between the Pd particles and the graphene pieces enable selective hydrogenation on Pd/h-NC catalyst with high activity.[8, 9, 50]

The active centers that weakly bind dissociated hydrogen species may exhibit high selectivity but they often have high activation energy for H_2 dissociation since the activation energy of a reaction is usually inversely proportional to the adsorption strength of the intermediates, limiting the activity of these catalysts.[8, 50, 51] In order to unravel the nature of H_2 activation on the h-NC supported Pd particles, we conducted the hydrogen oxidation experiment on the Pd/h-NC and Pd/XC-72 catalysts. In the temperature range of 20 °C to 50 °C, the H_2 reaction rate on the Pd/h-NC is much higher than that on the Pd/XC-72 (Figure S11 a-b). The activation energy (E_a) of H_2 oxidation on the Pd/h-NC is 11 kJ/mol while the E_a of the Pd/XC-72 is 31 kJ/mol, clearly suggesting that the h-NC supported Pd nanoparticles can much more easily dissociate H_2. From the above experiments we conclude that when compared with that on the Pd/XC-72, the synthesized Pd/h-NC catalyst provides more activated and weakly bound hydrogen species. As a result, the Pd/h-NC catalyst exhibits the excellent activity and selectivity for selective hydrogenation of 3-nitrostyrene.

In summary, we developed a mesoporous nanocarbon supported Pd nanoparticle catalyst for selective hydrogenation of the C=C bond in the presence of $-NO_2$ (selective hydrogenation of 3-nitrostyrene). The presence of high number density edge/defect sites in the synthesized h-NCs enhances the interaction between Pd species and the carbon support, resulting in electron transfer from Pd to carbon and thus forming a strong Pd-C bond. Such strong electronic interaction not only enables facile H_2 dissociation but also enhances the diffusion of the dissociated H species. The synthesized Pd/h-NC catalyst yielded a selectivity of 97%, stable up to 4 cycles, and a TOF of 21,845 /h for selective hydrogenation of 3-nitrostyrene to 3-ethylnitrobenzene, more than 80 times higher than that of the best catalyst reported in literature.[23] This work provides insights in understanding the effect of anchoring metal nanoparticles by edge/defect sites in carbon supports on selective hydrogenation reactions. The strategy of engineering carbon edge/defect sites to anchor Pd nanoparticles to tune catalytic

properties can be applied to other types of metals for various types of catalytic reactions.

This work was supported by the National Science Foundation under CHE-1465057. The authors gratefully acknowledge the use of facilities within the Eyring Materials Center and the John M. Cowley Center for High Resolution Electron Microscopy at Arizona State University.

Notes and references

1 A. Corma and P. Serna, *Science*, 2006, **313**, 332-334.
2 G. Booth, *Ullmann's Encyclopedia of Industrial Chemistry*, Wiley-VCH: Weinheim, 2012, Chapter 2.
3 H. U. Blaser, H. Steiner and M. Studer, *ChemCatChem*, 2009, **1**, 210-221.
4 L. Huang, P. Luo, W. Pei, X. Liu, Y. Wang, J. Wang, W. Xing and J. Huang, *Adv. Syn. Catal.*, 2012, **354**, 2689-2694.
5 M. Armbrüster, M. Behrens, F. Cinquini, K. Föttinger, Y. Grin, A. Haghofer, B. Klötzer, A. Knop-Gericke, H. Lorenz, A. Ota, S. Penner, J. Prinz, C. Rameshan, Z. Révay, D. Rosenthal, G. Rupprechter, P. Sautet, R. Schlögl, L. Shao, L. Szentmiklósi, D. Teschner, D. Torres, R. Wagner, R. Widmer and G. Wowsnick, *ChemCatChem*, 2012, **4**, 1048-1063.
6 A. Borodziński and G. C. Bond, *Catal. Rev.*, 2006, **48**, 91-144.
7 M. Chen, D. Kumar, C. W. Yi and D. W. Goodman, *Science*, 2005, **310**, 291-293.
8 F. R. Lucci, M. T. Darby, M. F. Mattera, C. J. Ivimey, A. J. Therrien, A. Michaelides, M. Stamatakis and E. C. Sykes, *J. Phys. Chem. Lett.*, 2016, **7**, 480-485.
9 G. Kyriakou, M. B. Boucher, A. D. Jewell, E. A. Lewis, T. J. Lawton, A. E. Baber, H. L. Tierney, M. Flytzani-Stephanopoulos and E. C. H. Sykes, *Science*, 2012, **335**, 1209-1212.
10 F. R. Lucci, M. D. Marcinkowski, T. J. Lawton and E. C. H. Sykes, *The J. Phys. Chem. C*, 2015, **119**, 24351-24357.
11 H. Wei, Y. Ren, A. Wang, X. Liu, X. Liu, L. Zhang, S. Miao, L. Li, J. Liu, J. Wang, G. Wang, D. Su and T. Zhang, *Chem. Sci.*, 2017, **8**, 5126-5131.
12 M. Makosch, W. I. Lin, V. Bumbálek, J. Sá, J. W. Medlin, K. Hungerbühler and J. A. van Bokhoven, *ACS Catal.*, 2012, **2**, 2079-2081.
13 K. Möbus, D. Wolf, H. Benischke, U. Dittmeier, K. Simon, U. Packruhn, R. Jantke, S. Weidlich, C. Weber and B. Chen, *Top. Catal.*, 2010, **53**, 1126-1131.
14 S. Furukawa, Y. Yoshida and T. Komatsu, *ACS Catal.*, 2014, **4**, 1441-1450.
15 A. Corma, P. Serna, P. Concepcion and J. J. Calvino, *J. Am. Chem. Soc.*, 2008, **130**, 8748-8753.
16 M. Boronat, P. Concepcion, A. Corma, S. Gonzalez, F. Illas and P. Serna, *J. Am. Chem. Soc.*, 2007, **129**, 16230-16237.
17 D. S. Su, G. Wen, S. Wu, F. Peng and R. Schlogl, *Angew. Chem. Int. Ed.*, 2017, **56**, 936-964.
18 J. Zhu, A. Holmen and D. Chen, *ChemCatChem*, 2013, **5**, 378-401.
19 S. A. Park, D. S. Kim, T. J. Kim and Y. T. Kim, *ACS Catal.*, 2013, **3**, 3067-3074.
20 T. W. Ebbesen and T. Takada, *Carbon*, 1995, **33**, 973-978.
21 J. C. Charlier, *Acc. Chem. Res.*, 2002, **35**, 1063-1069.
22 V. Lordi, N. Yao and J. Wei, *Chem. Mater.*, 2001, **13**, 733-737.
23 M. J. Beier, J. M. Andanson and A. Baiker, *ACS Catal.*, 2012, **2**, 2587-2595.
24 J. Liu, *Chin. J. Catal.*, 2017, **38**, 1460-1472.
25 J. Xia, G. He, L. Zhang, X. Sun and X. Wang, *Appl. Catal. B: Environ.*, 2016, **180**, 408-415.
26 B. Qiao, A. Wang, X. Yang, L. F. Allard, Z. Jiang, Y. Cui, J. Liu, J. Li and T. Zhang, *Nat. Chem.*, 2011, **3**, 634-641.
27 X. F. Yang, A. Q. Wang, B. T. Qiao, J. Li, J. Y. Liu and T. Zhang, *Acc. Chem Res*, 2013, **46**, 1740-1748.
28 J. Y. Liu, *ACS Catal.*, 2017, **7**, 34-59.
29 B. C. Gates, M. Flytzani-Stephanopoulos, D. A. Dixon and A. Katz, *Catal. Sci. Technol.*, 2017, **7**, 4259-4275.
30 A. Wang, J. Li and T. Zhang, Nat. Rev. Chem., 2018, **2**, 65-81.
31 M. M. Trandafir, L. Pop, N. D. Hădade, M. Florea, F. Neaţu, C. M. Teodorescu, B. Duraki, J. A. van Bokhoven, I. Grosu, V. I. Pârvulescu and H. Garcia, *Catal. Sci. Technol.*, 2016, **6**, 8344-8354.
32 T. Ishida, Y. Onuma, K. Kinjo, A. Hamasaki, H. Ohashi, T. Honma, T. Akita, T. Yokoyama, M. Tokunaga and M. Haruta, *Tetrahedron*, 2014, **70**, 6150-6155.
33 R. G. Rao, R. Blume, T. W. Hansen, E. Fuentes, K. Dreyer, S. Moldovan, O. Ersen, D. D. Hibbitts, Y. J. Chabal, R. Schlogl and J. P. Tessonnier, *Nat. Commun.*, 2017, **8**, 340.
34 A. Sadezky, H. Muckenhuber, H. Grothe, R. Niessner and U. Pöschl, *Carbon*, 2005, **43**, 1731-1742.
35 F. Tuinstra and J. L. Koenig, *J. Compos. Mater.*, 1970, **4**, 492-499.
36 A. C. Ferrari and J. Robertson, *Phys. Rev. B*, 2000, **61**, 14095-14107.
37 K. Teii, S. Shimada, M. Nakashima and A. T. H. Chuang, *J. Appl. Phys.*, 2009, **106**.
38 L. Wang, Z. Sofer, D. Bousa, D. Sedmidubsky, S. Huber, S. Matejkova, A. Michalcova and M. Pumera, *Angew. Chem. Int. Ed.*, 2016, **55**, 13965-13969.
39 G. Wen, B. Wang, C. Wang, J. Wang, Z. Tian, R. Schlogl and D. S. Su, *Angew. Chem. Int. Ed.*, 2017, **56**, 600-604.
40 J. H. Zhong, J. Zhang, X. Jin, J. Y. Liu, Q. Li, M. H. Li, W. Cai, D. Y. Wu, D. Zhan and B. Ren, *J. Am. Chem. Soc*, 2014, **136**, 16609-16617.
41 L. G. Cançado, K. Takai, T. Enoki, M. Endo, Y. A. Kim, H. Mizusaki, A. Jorio, L. N. Coelho, R. Magalhães-Paniago and M. A. Pimenta, *Appl. Phys. Lett.*, 2006, **88**, 163106.
42 I. Efremenko, *J. Catal.*, 2003, **214**, 53-67.
43 T. Prasomsri, D. Shi and D. E. Resasco, *Chem. Phys. Lett.*, 2010, **497**, 103-107.
44 F. Cárdenas-Lizana, Y. Hao, M. Crespo-Quesada, I. Yuranov, X. Wang, M. A. Keane and L. Kiwi-Minsker, *ACS Catal.*, 2013, **3**, 1386-1396.
45 Y. Lou, J. Ma, W. D. Hu, Q. G. Dai, L. Wang, W. C. Zhan, Y. L. Guo, X. M. Cao, Y. Guo, P. Hu and G. Z. Lu, *ACS Catal.*, 2016, **6**, 8127-8139.
46 R. Rahul, R. K. Singh, B. Bera, R. Devivaraprasad and M. Neergat, *Phys. Chem. Chem. Phys.*, 2015, **17**, 15146-15155.
47 Z. Zhao, X. Huang, M. Li, G. Wang, C. Lee, E. Zhu, X. Duan and Y. Huang, *J. Am. Chem. Soc*, 2015, **137**, 15672-15675.
48 Y. Feng, L. Zhou, Q. Wan, S. Lin and H. Guo, *Chem. Sci.*, 2018, **9**, 5890-5896.
49 K. Namba, S. Ogura, S. Ohno, W. Di, K. Kato, M. Wilde, I. Pletikosic, P. Pervan, M. Milun and K. Fukutani, *Proc. Natl. Acad. Sci. U S A*, 2018, **115**, 7896-7900.
50 J. K. Nørskov, T. Bligaard, A. Logadottir, S. Bahn, L. B. Hansen, M. Bollinger, H. Bengaard, B. Hammer, Z. Sljivancanin, M. Mavrikakis, Y. Xu, S. Dahl and C. J. H. Jacobsen, *J. Catal.*, 2002, **209**, 275-278.
51 B. Hammer and J. K. Norskov, *Nature*, 1995, **376**, 238-240.

Table of Contents

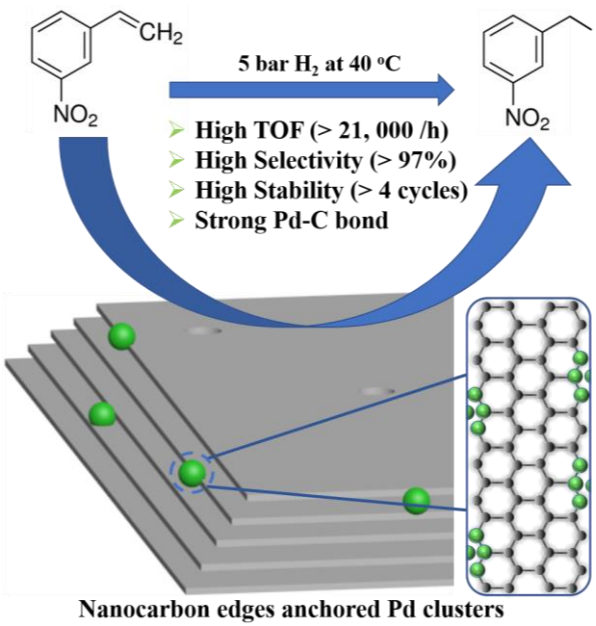

Nanocarbon edges anchored Pd clusters